Towards Resolving Fiber Crossings with Higher Order Tensor Inpainting

Thomas Schultz

Abstract The use of second-order tensors for the modeling of data from Diffusion Weighted Magnetic Resonance Imaging (DW-MRI) is limited by their inability to represent more than one dominant direction in cases of crossing fiber bundles or partial voluming. Higher-order tensors have been used in High Angular Resolution Diffusion Imaging (HARDI) to overcome these problems, but their larger number of parameters leads to longer measurement times for data acquisition. In this work, we demonstrate that higher-order tensors that indicate likely fiber directions can be estimated from a small number of diffusion-weighted measurements by taking into account information from local neighborhoods. To this end, we generalize tensor voting, a method from computer vision, to higher-order tensors. We demonstrate that the resulting even-order tensor fields facilitate fiber reconstruction at crossings both in synthetic and in real DW-MRI data, and that the odd-order fields differentiate crossings from junctions.

1 Introduction

Diffusion Weighted Magnetic Resonance Imaging (DW-MRI) is a medical imaging modality that allows for a non-invasive investigation of fibrous tissue, such as the nerve fiber bundles in the human brain [1]. In cases where a clear principal fiber direction exists, it is generally well-aligned with the main diffusion direction captured by the second-order diffusion tensor (DT-MRI) model [2]. However, DT-MRI provides insufficient information in cases of partial voluming and crossing or spreading fiber bundles. High Angular Resolution Diffusion Imaging (HARDI) uses

T. Schultz (✉)
University of Chicago, Computation Institute, 5735 S. Ellis Ave #209A, Chicago, IL, 60637, USA
e-mail: tschultz@tuebingen.mpg.de

D.H. Laidlaw and A. Vilanova (eds.), *New Developments in the Visualization and Processing of Tensor Fields*, Mathematics and Visualization,
DOI 10.1007/978-3-642-27343-8_13,

more complex models like higher-order tensors [3, 4], but requires a larger number of measurements, which are usually too time-consuming in a clinical context.

Inpainting is a process by which a damaged image is restored, or an object is removed from an image in an unobtrusive way. Different strategies have been developed to fill in the missing information in such cases in an automated manner. They can be classified roughly into structure-based methods, which try to continue the surrounding image geometry into the missing region [5] and texture synthesis approaches, that generate patches from statistical models [6] or by copying pixels from example images [7].

Our work is motivated by the observation that the image inpainting problem resembles the problem of complex fiber configurations in DT-MRI data: In both cases, information is missing in certain regions of a dataset. Our goal is to use ideas from inpainting in a preprocess that facilitates fiber tracking through such complex regions. Our method belongs to the class of techniques that fill in small holes by continuing existing structures in the neighborhood. It is based on tensor voting, an approach from computer vision that can be used to infer likely continuations of lines, and that we extend to higher-order tensors in order to preserve directional information at crossings.

This chapter is structured as follows: After reviewing related work in Sect. 2, we will introduce the concept of higher-order tensor voting in Sect. 3. In Sect. 4, we explain the application of this method to the problem of estimating tensors that can be used for fiber tracking. Finally, results are presented in Sect. 5 and the paper is concluded in Sect. 6.

2 Related Work

Tensor voting [8] is a framework for perceptual organization. Based on principles of human perception, it tries to group tokens (like points, lines, or surface segments) into structures that appear natural to a human observer. The method was first proposed for the automated detection of perceptual contours [9], but has been extended to numerous other applications, including the inpainting problem [10].

Our work differs from this existing use of tensor voting for inpainting in that our input is a three-dimensional second-order tensor field rather than a two-dimensional color image. The formulation of texture synthesis as a tensor voting problem, which is one of the main contributions of [10], does not apply to our problem. Instead, we extend tensor voting by using higher-order tensors to represent directional information at crossings.

Inpainting small image regions is closely related to image interpolation. Weickert and Welk [11] have developed a PDE-based method for interpolation of second-order tensor fields. As part of our experiments, we successfully applied their approach to higher-order tensor fields. However, we found that tensor voting makes it easier to re-orient the propagated tensors and, in our particular application, allows for a simpler, non-iterative, and relatively fast implementation. A comparison

between tensor voting and PDE-based methods in a different context is presented by Moreno et al. in Chap. 9 of this book.

The higher-order tensors generated by our method are similar to the "tractosemas" proposed by Barmpoutis et al. [12] and the "extrapolated spherical diffusion functions" by Prčkovska [13] in that they do not have an immediate physical meaning, but are designed to indicate likely fiber directions. However, the main purpose of [12] is to create distributions from HARDI data which are no longer antipodally symmetric. Even though Sect. 5.3 will demonstrate that asymmetries can also be detected by tensor voting, our focus is to infer information about crossings from data with low angular resolution.

A study by Caan et al. [14] has pursued a similar goal, but under different conditions: They acquire low angular resolution data from different subjects, and estimate a high angular resolution atlas from the coregistered results. In contrast, our method takes its information from spatial neighborhoods rather than a cohort of subjects and thus works on individual datasets.

Previous work that integrates neighborhood information into the fiber tracking process includes the tensorlines algorithm by Weinstein et al. [15]. However, it only uses information from the previous tracking step, while our voting process takes the full neighborhood into account.

The spin glass model by Mangin et al. [16] aims at balancing local diffusion directions with global curvature constraints by simulating coupled compass needles in a magnetic field which is defined from the diffusion tensors. Even though a simple synthetic crossing has been resolved using a two-compass variant [17], it has not been applied to curved tracts, and results on real data have only been presented based on a single-compass model that does not support crossings [16].

An alternative voting-based approach to tractography, inspired by the Hough transform, was recently presented by Aganj et al. [18]. They identify the most plausible fiber trajectories by voting on a large number of possible curves, while our method votes on local fiber directions and does a tractography only in a subsequent step. Since [18] is only an extended abstract, it does not provide enough detail for a reproduction and side-by-side comparison of results.

3 Higher-Order Tensor Voting

3.1 Basics of Tensor Voting

The input of the tensor voting algorithm is a set of tokens. Even though tensor voting allows for different types of tokens, like unoriented points and curve or surface elements, we are specifically interested in reconstructing the trajectories of major nerve fiber bundles, so we only make use of the part of the framework that deals with curves.

In tensor voting, each curve element generates hypotheses about likely continuations and votes for them. Individual votes encode the direction of the proposed

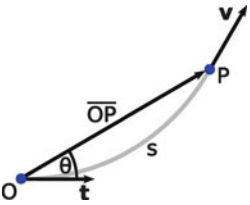

Fig. 1 Given two points O and P along with a tangent **t** at O, tensor voting considers the osculating circle (*gray*) to be their most likely connection, leading to the inferred tangent **v** at P

curve, and a scalar saliency, indicating the confidence that the voter has in it. In a subsequent step, the accumulated votes are analyzed to identify the curve for which all input tokens together provide the strongest evidence. Accumulated votes reflect the overall saliency, the average direction, weighted by individual saliencies, and the spread around it.

For a curve element given by a point O and a tangent direction **t**, tensor voting assumes that the most likely continuation that includes a second point P is an arc of their osculating circle, i.e., the circle that passes through both O and P and shares the tangent **t** at O (cf. Fig. 1). Consequently, the direction of the vote cast from O to P is the tangent **v** of the osculating circle at that point. The saliency of the vote decreases both with arc length s and with the curvature κ of the circle. If the angle θ between **t** and the line $\overline{\text{OP}}$ exceeds 45°, the saliency is set to zero. A detailed justification of these choices is given in [19].

3.2 Introducing Higher-Order Tensors

In the original framework, votes are represented by second-order tensors with sorted eigenvalues $\lambda_1 \geq \lambda_2 \geq \lambda_3 \geq 0$. The relative magnitudes of the eigenvalues reflect the type of a structure, the eigenvector directions describe its orientation.

Our implementation deviates from the established tensor voting algorithm in two ways: First, curve elements are traditionally encoded as planar tensors ($\lambda_1 = \lambda_2 \gg \lambda_3$) whose larger eigenvector pair spans the normal plane. In contrast, we let the major eigenvector represent the tangent direction. This agrees with the role of the principal eigenvector in DT-MRI, which is assumed to be tangential to the fiber trajectory, and it allows us to use simple stick votes for curves, which are the only relevant elements in our application.

Second, traditional tensor voting represents crossings and junctions as isotropic tensors ($\lambda_1 = \lambda_2 = \lambda_3$), which do not possess any directional information. Since it is the main motivation of our work to overcome the inability of DT-MRI to resolve the involved fiber directions at crossings, we replace the second-order tensors with a higher-order tensor representation, which retains directional information even when averaging differently oriented stick tensors. This is done in analogy to the higher-order structure tensors in [20] and is illustrated in Fig. 2.

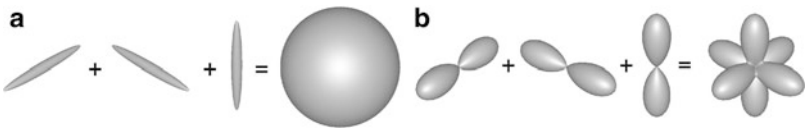

Fig. 2 When adding orthogonal second-order tensors, the result has no directional information (**a**). In the sixth-order case, the orientations of the individual terms is reflected in the sum (**b**). Therefore, we use higher-order tensors in our voting

3.3 Formalizing the Voting Process

The votes in our algorithm are created in three steps: First, the correct direction is determined and represented as a unit vector $\mathbf{v}$. Then, the scalar saliency ψ is computed. Finally, a higher-order tensor vote $\mathcal{V}$ is formed by a repeated outer product of $\mathbf{v}$ with itself, scaled with saliency ψ.

The first two steps are analogous to the traditional creation of stick votes [19]: Let θ be the angle between the tangent $\mathbf{t}$ at O and the vector $\overline{\mathrm{OP}}$ (Fig. 1). Then, $\mathbf{v}$ is the tangent of the osculating circle at P, and is created by rotating $\mathbf{t}$ by the angle 2θ around the axis given by $\mathbf{t} \times \overline{\mathrm{OP}}$. Thus, $\mathbf{t}$, $\mathbf{v}$, and $\overline{\mathrm{OP}}$ lie in a common plane.

Saliency decreases with arc length s and curvature κ:

$$s = \frac{\theta \|\overline{\mathrm{OP}}\|}{\sin\theta} \qquad \kappa = \frac{2\sin\theta}{\|\overline{\mathrm{OP}}\|} \tag{1}$$

The voting has two main parameters: σ determines how rapidly saliency decays with distance, ρ controls the decay with curvature. If $\theta > 45°$, the saliency ψ is set to zero. Otherwise, it is given as

$$\psi(s,\kappa) = e^{-\frac{s^2}{\sigma^2} - \frac{\kappa^2}{\rho^2}}. \tag{2}$$

In the original tensor voting approach, ρ is set as a function of σ, based on the assumption that it is equally plausible to join two orthogonal curve elements with a smooth curve or a sharp corner [9]. In fiber tracking, it is commonly assumed that fiber bundles do not bend sharply [21]. Therefore, we penalize curvature more than regular tensor voting would. This is achieved by fixing $\sigma = 2$ and $\rho = 0.3$.

With these ingredients, the final vote is computed as $\mathcal{V} = \psi(s,\kappa)\mathbf{v}^{\otimes l}$, where $\mathbf{v}^{\otimes l}$ denotes taking the outer product of $\mathbf{v}$ with itself l times. In component notation,

$$[\mathcal{V}]_{i_1 i_2 \ldots i_l} = \psi(s,\kappa) v_{i_1} v_{i_2} \cdots v_{i_l}. \tag{3}$$

Since $\mathcal{V}$ is invariant under arbitrary index permutations, it is sufficient to store a small number of non-redundant components (cf. [20]). All presented experiments use tensor order $l = 6$, which has been found sufficient to resolve intersections of three fiber bundles [22].

3.4 Analyzing the Accumulated Votes

Individual votes are accumulated by simple component-wise addition of the respective tensors. In traditional tensor voting, the resulting tensor $\mathbf{T}$ is analyzed via its spectral decomposition into eigenvalues $\lambda_1 \geq \lambda_2 \geq \lambda_3$ and eigenvectors $\mathbf{e}_1$, $\mathbf{e}_2$, $\mathbf{e}_3$:

$$\mathbf{T} = \sum_{i=1}^{3} \lambda_i \mathbf{e}_i \otimes \mathbf{e}_i \tag{4}$$

From this, a stick, plate, and a ball component are detected with saliencies

$$\psi_s = \lambda_1 - \lambda_2, \quad \psi_p = \lambda_2 - \lambda_3, \quad \psi_b = \lambda_3 \tag{5}$$

respectively. No exact equivalent of the spectral decomposition exists for the higher-order case, but a previous work [22] proposed an algorithm to approximate a given order-l tensor $\mathscr{T}$ with a sum of symmetric rank-1 terms:

$$\mathscr{T} \approx \sum_{i=1}^{r} \lambda_i \mathbf{e}_i^{\otimes l} \tag{6}$$

Here, the vectors $\mathbf{e}_i$ are still unit-length, but no longer pairwise orthogonal. The rank-1 terms $\mathbf{e}_i^{\otimes l}$ correspond to stick components, and represent curve elements in our modified tensor voting framework. Since equally large $\lambda_1 \approx \lambda_2$ can now indicate two salient stick components in different directions, we can no longer rely on the difference $\lambda_1 - \lambda_2$ to define saliency, as in Eq. (5). Rather, we assign high saliency to a direction if the tensor's homogeneous form

$$T(\mathbf{v}) = \mathscr{T} \cdot^l \mathbf{v} = \sum_{i_1, i_2, \ldots, i_l} [\mathcal{T}]_{i_1 i_2 \ldots i_l} v_{i_1} v_{i_2} \cdots v_{i_l}, \tag{7}$$

as it is plotted in Fig. 2b, has large convex curvature in that direction.

Restrict $T(\mathbf{v})$ to the unit sphere and let $\mathbf{H}_i$ be the symmetric 2×2 Hessian matrix of second derivatives of $T(\mathbf{v})$ on the sphere, evaluated at the curve direction $\mathbf{e}_i$ that was estimated in Eq. (6). This Hessian can be obtained either numerically [23] or analytically, by expressing $T(\mathbf{v})$ in spherical coordinates [24]. Let $\mu_1 \geq \mu_2$ be the sorted eigenvalues of $\mathbf{H}_i$. If $\mathbf{e}_i$ is a salient stick component, we expect $T(\mathbf{v})$ to be strongly convex ($\mu_1 \ll 0$), so we measure saliency ψ as

$$\psi = -\frac{\mu_1}{l}. \tag{8}$$

The normalization by tensor order l ensures that the maximum saliency of component $\mathbf{e}_i^{\otimes l}$ is given by $\psi = \lambda_i$. In case of the second-order tensors used in traditional tensor voting, $\mu_1 = 2(\lambda_2 - \lambda_1)$. Therefore, the definition of ψ in Eq. (8) is equivalent to ψ_s in Eq. (5) in this case.

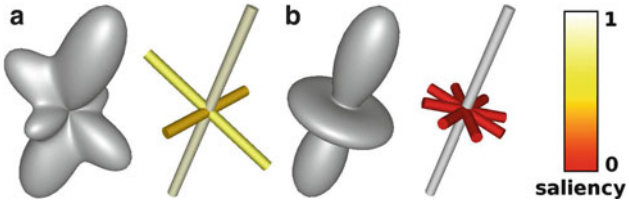

Fig. 3 Accumulated higher-order votes are approximated with a sum of rank-1 terms that represent stick components. In Subfigure (**a**), all three contributions have significant saliency, as computed according to Eq. (8) from the convex shape in these directions. In (**b**), the planar contribution orthogonal to the main direction is decomposed into three sticks with zero saliency

Figure 3a illustrates that a single accumulated higher-order tensor vote can contain multiple stick components, with different angles and saliencies. The plate component in Fig. 3b can be subdivided further into four rank-1 terms, but they have zero saliency as stick components. This is completely analogous to second-order plate tensors, which can be written as $\mathbf{e}_1 \otimes \mathbf{e}_1 + \mathbf{e}_2 \otimes \mathbf{e}_2$ for any two orthonormal vectors $\mathbf{e}_1$ and $\mathbf{e}_2$ that span the plane.

4 Inpainting as a Preprocess for Tractography

Fiber tracking [25], also known as tractography [21], infers likely fiber trajectories by computing integral curves which are everywhere tangential to the major eigenvector of the diffusion tensor field. Tracking is stopped when the difference $\lambda_1 - \lambda_2$ between the larger two eigenvalues becomes too small, since this typically indicates that the diffusion tensor no longer represents a single homogeneous fiber bundle. A common criterion is the linearity measure of Westin et al. [26],

$$c_l = \frac{\lambda_1 - \lambda_2}{\lambda_1}. \tag{9}$$

In our experiments, we stop when $c_l < 0.4$.

In order to use tensor voting as a preprocess for fiber tracking, we need to define a set of tokens that generate the votes, and to mark the region in which the inpainting should happen. Tokens are placed in all voxels where c_l is large enough for fiber tracking. Their direction is given by the principal eigenvector of the diffusion tensor. In analogy to streamline tractography, which makes a hard binary decision about whether or not to follow an eigenvector direction, our method assigns the same saliency to all input tokens. The inpainting mask is given by the voxels in which c_l is too low for fiber tracking. Information from the neighborhood is propagated into the inpainting region by the tensor voting process described in Sect. 3.

Outside the mask, tokens are represented as rank-1 tensors, as given by Eq. (3). To keep the norm of tensors within and outside the mask in a comparable range, we scale all votes by $2/\iiint \psi$, where $\iiint \psi$ denotes the integral of ψ from Eq. (2) over three-dimensional space. In practice, we evaluate the integral numerically over a spatial neighborhood where $\psi > 0.01$.

Fiber tracking is performed on the resulting higher-order tensor field using the algorithm from [22]. Voxels outside the brain are marked a priori based on their low MR signal, and are not taken into account at any point. Setting up the inpainting does not involve any new parameters, since the threshold on c_l is taken from the algorithm for DT-MRI tractography. However, the higher-order tracking process needs a termination criterion; in our examples, we stop when no rank-1 contribution with $\psi > 0.01$ is found within 20° of the current tracking direction.

5 Results

In order to validate our method, we have applied it to three synthetic datasets. They were created by modeling fiber crossings as a mixture of second-order diffusion tensors with fractional anisotropy FA $= 0.87$ [27], by simulating diffusion-weighted images (DWIs) from them, and estimating a DT-MRI model through a linearized least squares fit [2]. DWIs were simulated in 12 evenly distributed directions, with a b-value of $b = 1{,}000\,\mathrm{s/mm^2}$.

We also used our method for the reconstruction of a major fiber bundle in a real dataset of a healthy human brain. Like the synthetic data, it consisted of 12 diffusion-weighted images at $b = 1{,}000\,\mathrm{s/mm^2}$, plus one non-weighted image, and the same fitting procedure was used.

5.1 Results on Synthetic Data

Our first example is a crossing of two orthogonal fiber bundles. Figure 4 shows a superquadric glyph visualization [28] of the synthetic DT-MRI data (a), the inpainted higher-order tensor field (b), and a tractography based on the higher-order tensors (c). Our inpainting reconstructs this simple configuration perfectly.

As a more challenging test case, we created a second dataset in which a straight fiber bundle is intersected by a parabolic one. In Fig. 5a, a ground truth tractography is presented. It is based on a spherical deconvolution model [29] that has been computed from simulated HARDI measurements (60 directions, $b = 1{,}000\,\mathrm{s/mm^2}$). In all examples, the tracking is seeded at the top and at the left side of the image.

Since the parabolic shape violates the constant curvature assumption made by the tensor voting approach, the curved bundle is not reconstructed perfectly in this case; however, the correct connectivity is still inferred in a large part of the bundle (b). For comparison, Subfigure (c) demonstrates that the tensorlines algorithm [15], a previous approach that integrates neighborhood information in the fiber tracking process, fails completely to reconstruct the crossing.

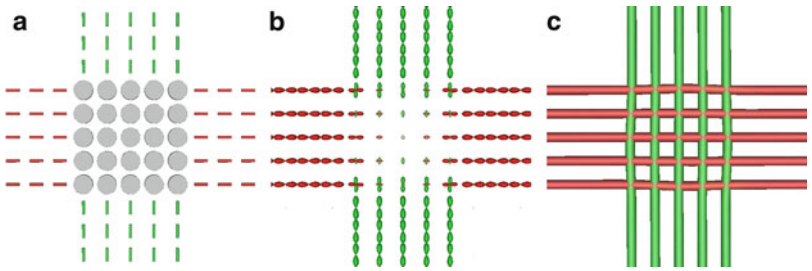

Fig. 4 At a 90° crossing, second-order tensors become planar, preventing fiber tracking (**a**). Our inpainting process infers higher-order tensors (**b**) that allow for a reconstruction of the crossing (**c**)

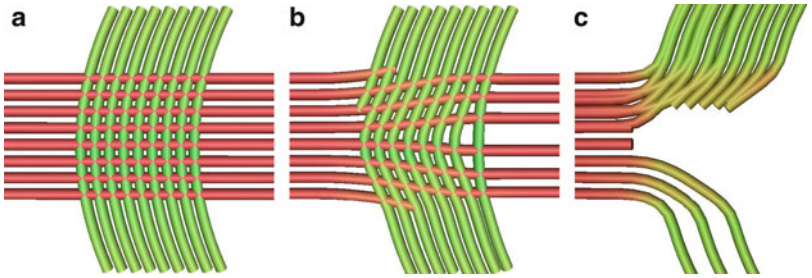

Fig. 5 Since the parabolic (*green*) fibers in (**a**) violate the constant curvature assumption of tensor voting, which was illustrated in Fig. 1, our inpainting produces imperfect results, but is still able to infer the correct connectivity (**b**). The tensorlines algorithm is unable to resolve the crossing (**c**)

5.2 Result on Real Data

In the real dataset, we aimed at tracking the left pyramidal tract by seeding in the internal capsule. Due to its high importance to motor function, reconstructions of this tract have been used repeatedly for surgical planning [30–32].

With second-order diffusion tensors alone, it is difficult to capture the bundle in its entirety, since c_l drops when the tract crosses the transcallosal fibers that run through the corpus callosum (Fig. 6a, red ellipse). As shown in Fig. 6b, higher-order tensor inpainting successfully bridges this gap, and allowed us to continue the tracking towards the cortical surface.

5.3 Distinguishing Crossings from Junctions

Recently, Barmpoutis et al. [12] have employed a diffusion process to create a field of asymmetric spherical functions that differentiate between X-shaped crossings and Y-shaped junctions. To illustrate that the same distinction can also be made via a tensor voting, we have created a synthetic junction, shown in Fig. 7a.

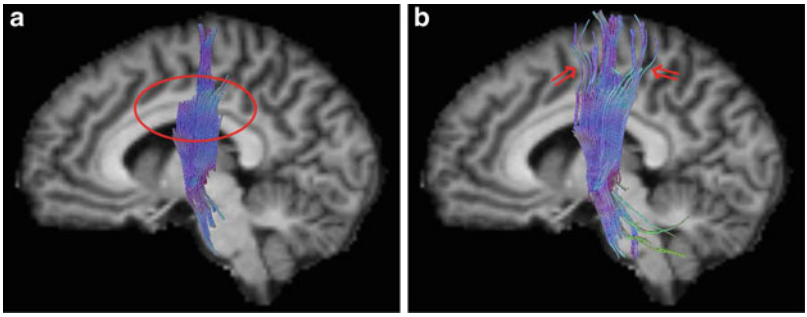

Fig. 6 Due to crossing transcallosal fibers, tracking of the pyramidal tract in this DT-MRI dataset ended prematurely (**a**). Higher-order tensor inpainting allowed the tracking to continue towards the cortex (**b**)

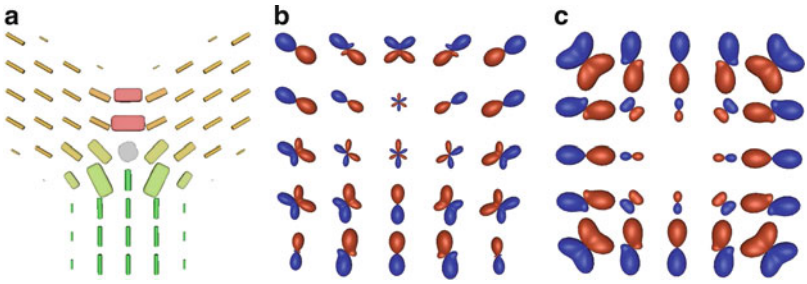

Fig. 7 The direction and polarity of fibers meeting in a 120° junction (**a**) is clearly shown by third-order tensor votes (**b**, closeup), whose homogeneous forms are antisymmetric (*blue* indicates negative values, *red* positive). At the center of crossings, odd-order tensor votes cancel out (**c**), effectively distinguishing crossings from junctions

In order to find the location and polarity of boundaries, Tong et al. [33] extend the traditional second-order tensor voting framework towards vectors ("first-order tensors"): Regions in the center of a structure will receive vector votes from both sides, which cancel out due to their opposite orientation. At structure boundaries, however, vector votes accumulate.

This approach does not carry over to our problem directly, since vectors cancel out both at crossings and at regular (e.g., 120° triple) junctions. However, we observe that tensors of odd order $l \geq 3$ still cancel out at crossings, while they have non-zero norm and indicate the directions of the involved bundles at junctions.

This is because the homogeneous form $T(\mathbf{v})$ that characterizes a symmetric tensor (Eq. 7) is antipodally antisymmetric $T(-\mathbf{v}) = -T(\mathbf{v})$ for odd l, but can become multimodal for $l \geq 3$. Odd-order votes are generated in complete analogy to even-order ones (cf. Sect. 3.3).

Figure 7b, c plot the homogeneous forms of accumulated third-order tensor votes; blue indicates positive values, red negative ones. The glyph at the center of the junction (b) clearly indicates the directions and polarities of the three joining

bundles. At the center of crossings (c), odd-order votes cancel out; the directions of the involved bundles is instead given by the even-order votes (Fig. 4b).

Taken together, even-order (antipodally symmetric) and odd-order (antipodally antisymmetric) tensors hold all the information that is present in general asymmetric functions on the sphere, as they are used in [12].

6 Conclusion and Future Work

In this chapter, we have made two contributions. First, we have introduced higher-order tensor voting, an extension of the standard tensor voting method that allows one to preserve directional information at crossings and junctions. We expect that higher-order tensor voting will also prove useful in other applications. However, to leverage the full framework, rather than being restricted to inferring curves, more research is required on decompositions of totally symmetric higher-order tensors.

Second, we have approached the problem of missing information in DT-MRI due to partial voluming from a new perspective, by treating it in analogy to image inpainting. For this, we have relied on generic rules of what constitutes a good continuation of a curve. They are encoded in the tensor voting algorithm and include proximity, similarity, and simplicity [19]. In the future, one might consider exploiting more specific prior knowledge about likely continuations of fiber bundles, which could be given in the form of a HARDI brain atlas. While we have concentrated on structure-inferring inpainting in this work, such an approach could take inspiration from example-based texture synthesis [7].

It is not the goal of our research to establish inpainting as an alternative to HARDI. However, our results indicate that in cases where the acquisition of high angular resolution data cannot be afforded, inpainting can help with the extraction of clinically relevant fiber tracts.

As part of our future work, we would like to employ tensor voting techniques similar to the one described in this chapter to stabilize the tracking process in cases where HARDI data is available, and exploit the antisymmetric information provided by odd-order tensor votes.

Acknowledgements I would like to thank Alfred Anwander (MPI CBS, Leipzig, Germany) for providing the DW-MRI dataset that was used to create Fig. 6. This work was supported by a fellowship within the Postdoc Program of the German Academic Exchange Service (DAAD).

References

1. Le Bihan, D., Breton, E., Lallemand, D., Grenier, P., Cabanis, E., Laval-Jeantet, M.: MR imaging of intravoxel incoherent motions: application to diffusion and perfusion in neurologic disorders. Radiology **161**, 401–407 (1986)
2. Basser, P.J., Mattiello, J., Le Bihan, D.: Estimation of the effective self-diffusion tensor from the NMR spin echo. J. Magn. Reson. B **103**, 247–254 (1994)

3. Özarslan, E., Mareci, T.: Generalized diffusion tensor imaging and analytical relationships between diffusion tensor imaging and high angular resolution diffusion imaging. Magn. Reson. Med. **50**, 955–965 (2003)
4. Liu, C., Bammer, R., Acar, B., Moseley, M.E.: Characterizing non-gaussian diffusion by using generalized diffusion tensors. Magn. Reson. Med. **51**, 924–937 (2004)
5. Bertalmio, M., Sapiro, G., Caselles, V., Ballester, C.: Image inpainting. In: Proceedings of ACM SIGGRAPH, New Orleans, pp. 417–424. ACM, New York (2000)
6. Portilla, J., Simoncelli, E.P.: A parametric texture model based on joint statistics of complex wavelet coefficients. Int. J. Comput. Vis. **40**, 49–71 (2000)
7. Efros, A.A., Leung, T.K.: Texture synthesis by non-parametric sampling. In: Proceedings of IEEE International Conference on Computer Vision (ICCV), Kerkyra, pp. 1033–1038. IEEE, Los Alamitos (1999)
8. Medioni, G., Lee, M.S., Tang, C.K.: A Computational Framework for Segmentation and Grouping. Elsevier, Amsterdam/New York (2000)
9. Guy, G., Medioni, G.: Inferring global perceptual contours from local features. Int. J. Comput. Vis. **20**, 113–133 (1996)
10. Jia, J., Tang, C.K.: Image repairing: robust image synthesis by adaptive ND tensor voting. In: IEEE Conference on Computer Vision and Pattern Recognition (CVPR), Madison, vol. 2, pp. 643–650. IEEE, Los Alamitos (2003)
11. Weickert, J., Welk, M.: Tensor field interpolation with PDEs. In: Weickert, J., Hagen, H. (eds.) Visualization and Processing of Tensor Fields, pp. 315–325. Springer, Berlin/Heidelberg (2006)
12. Barmpoutis, A., Vemuri, B.C., Howland, D., Forder, J.R.: Extracting tractosemas from a displacement probability field for tractography in DW-MRI. In: Metaxas D. et al. (eds.) Proceedings of Medical Image Computing and Computer-Assisted Intervention (MICCAI), New York. Lecture Notes in Computer Science, vol. 5241, pp. 9–16. Springer, Berlin/Heidelberg (2008)
13. Prčkovska, V.: High angular resolution diffusion imaging – processing & visualization. Ph.D. thesis, Technische Universiteit Eindhoven (2010)
14. Caan, M., Sage, C., van der Graaf, M., Grimbergen, C., Sunaert, S., van Vliet, L., Vos, F.: Dual tensor atlas generation based on a cohort of coregistered non-HARDI datasets. In: Yang, G.Z. et al. (eds.) Proceedings of Medical Image Computing and Computer-Assisted Intervention (MICCAI), London. Lecture Notes in Computer Science, vol. 5761, pp. 869–876. Springer, Berlin/Heidelberg (2009)
15. Weinstein, D., Kindlmann, G., Lundberg, E.: Tensorlines: advection-diffusion based propagation through diffusion tensor fields. In: Proceedings of IEEE Visualization, IEEE Computer Society Press, San Francisco, pp. 249–253 (1999)
16. Mangin, J.F., Poupon, C., Cointepas, Y., Rivière, D., Papadopoulos-Orfanos, D., Clark, C.A., Régis, J., Le Bihan, D.: A framework based on spin glass models for the inference of anatomical connectivity from diffusion-weighted MR data – a technical review. NMR Biomed. **15**, 481–492 (2002)
17. Cointepas, Y., Poupon, C., Le Bihan, D., Mangin, J.F.: A spin glass based framework to untangle fiber crossing in MR diffusion based tracking. In: Dohi, T., Kikinis, R. (eds.) Proceedings of Medical Image Computing and Computer-Assisted Intervention (MICCAI), Tokyo. Lecture Notes in Computer Science, vol. 2488, pp. 475–482. Springer, Berlin/Heidelberg (2002)
18. Aganj, I., Lenglet, C., Keriven, R., Sapiro, G., Harel, N., Thompson, P.: A Hough transform global approach to diffusion MRI tractography. In: Proceedings of International Society of Magnetic Resonance in Medicine (ISMRM), Honolulu, vol. 17, p. 854. The Society, Berkeley (2009)
19. Mordohai, P., Medioni, G.: Tensor voting: a perceptual organization approach to computer vision and machine learning. Morgan & Claypool, San Rafael (2007)
20. Schultz, T., Weickert, J., Seidel, H.P.: A higher-order structure tensor. In: Laidlaw, D.H., Weickert, J. (eds.) Visualization and Processing of Tensor Fields – Advances and Perspectives, pp. 263–280. Springer, Berlin/Heidelberg (2009)

21. Basser, P.J., Pajevic, S., Pierpaoli, C., Duda, J., Aldroubi, A.: In vivo fiber tractography using DT-MRI data. Magn. Reson. Med. **44**, 625–632 (2000)
22. Schultz, T., Seidel, H.P.: Estimating crossing fibers: a tensor decomposition approach. IEEE Trans. Vis. Comput. Graph. (Proc. IEEE Visualization) **14**, 1635–1642 (2008)
23. Seunarine, K.K., Cook, P.A., Hall, M.G., Embleton, K.V., Parker, G.J.M., Alexander, D.C.: Exploiting peak anisotropy for tracking through complex structures. In: Proceedings of IEEE Workshop Mathematical Methods in Biomedical Image Analysis (MMBIA), IEEE, Rio de Janeiro, Brazil, pp. 1–8 (2007)
24. Schultz, T., Kindlmann, G.: A maximum enhancing higher-order tensor glyph. Comput. Graph. Forum (Proc. EuroVis) **29**, 1143–1152 (2010)
25. Mori, S., Crain, B.J., Chacko, V.P., van Zijl, P.C.M.: Three-dimensional tracking of axonal projections in the brain by magnetic resonance imaging. Ann. Neurol. **45**, 265–269 (1999)
26. Westin, C.F., Maier, S., Khidhir, B., Everett, P., Jolesz, F., Kikinis, R.: Image processing for diffusion tensor magnetic resonance imaging. In: Proceedings of Medical Image Computing and Computer-Assisted Intervention (MICCAI), Cambridge. Lecture Notes in Computer Science, vol. 1679, pp. 441–452. Springer, Berlin/New York (1999)
27. Basser, P.J., Pierpaoli, C.: Microstructural and physiological features of tissues elucidated by quantitative-diffusion-tensor MRI. J. Magn. Reson. B **111**, 209–219 (1996)
28. Kindlmann, G.: Superquadric tensor glyphs. In: EG/IEEE Symposium on Visualization (SymVis), Eurographics Association, Konstanz, Germany, pp. 147–154 (2004)
29. Tournier, J.D., Calamante, F., Gadian, D.G., Connelly, A.: Direct estimation of the fiber orientation density function from diffusion-weighted MRI data using spherical deconvolution. NeuroImage **23**, 1176–1185 (2004)
30. Niizuma, K., Fujimura, M., Kumabe, T., Higano, S., Tominaga, T.: Surgical treatment of paraventricular cavernous angioma: fibre tracking for visualizing the corticospinal tract and determining surgical approach. J. Clin. Neurosci. **13**, 1028–1032 (2006)
31. Nimsky, C., Ganslandt, O., Enders, F., Merhof, D., Hammen, T., Buchfelder, M.: Visualization strategies for major white matter tracts for intraoperative use. Int. J. Comput. Assist. Radiol. Surg. **1**, 13–22 (2006)
32. Qazi, A.A., Radmanesh, A., O'Donnell, L., Kindlmann, G., Peled, S., Westin, C.F., Golby, A.J.: Resolving crossings in the corticospinal tract by two-tensor streamline tractography: method and clinical assessment using fMRI. NeuroImage **47**, T98–T106 (2009)
33. Tong, W.S., Tang, C.K., Mordohai, P., Medioni, G.: First order augmentation to tensor voting for boundary inference and multiscale analysis in 3D. IEEE Trans. Pattern Anal. Mach. Intell. **26**, 594–611 (2004)

http://www.springer.com/978-3-642-27342-1

New Developments in the Visualization and Processing of Tensor Fields

Laidlaw, D.H.; Vilanova, A. (Eds.)
2012, XXI, 384 p. 153 illus., 129 illus. in color.,
Hardcover
ISBN: 978-3-642-27342-1